*Article*

# Glaciogenic Periglacial Landform in the Making—Geomorphological Evolution of a Rockfall on a Small Glacier in the Horlachtal, Stubai Alps, Austria

Fabian Fleischer [1,*], Florian Haas [1], Moritz Altmann [1], Jakob Rom [1], Camillo Ressl [2] and Michael Becht [1]

1   Department of Physical Geography, Catholic University of Eichstätt-Ingolstadt, 95072 Eichstätt, Germany
2   Department of Geodesy and Geoinformation, Technische Universität Wien, 1040 Vienna, Austria
*   Correspondence: fabian.fleischer@ku.de

**Abstract:** Deglaciation in high mountain areas signifies the transition from glacial to periglacial conditioned landscapes. Due to the reduced melt rate of debris-covered glacier ice, these areas of the glacier may persist long after the surrounding glacier has melted, resulting in the formation of distinct post-glacial landforms. In this study, we examine the geomorphological evolution and potential future development of a 19,267 m$^3$ ± 204 m$^3$ rockfall from the permafrost-affected headwall on the low-elevated Zwieselbachferner in the Horlachtal, Stubai Alps, Austria. The analysis uses multi-epochal remote sensing data, including photogrammetrically and airborne laser scanning-derived digital elevation models, orthophotos, and satellite data, covering a period from the initial rockfall in 2003/2004 to 2022. The data reveals that the rockfall event resulted in the formation of a supraglacial debris layer of varying thickness, spanning an area of 15,920 m$^2$. Subsequently, 13 further rockfalls ranging from 67 m$^3$ ± 6 m$^3$ to 4250 m$^3$ ± 121 m$^3$ were detected. The mean ice thickness of the debris-covered area only slightly decreased between 2006 and 2022, in contrast to the surrounding glacier, whose thickness and length have strongly decreased. This results in the formation of a steep front and flanks that become increasingly covered by debris redistribution. The study suggests that the glacier ice covered by rockfall-derived debris will remain as a periglacial landform of glacial origin after the complete melting of the surrounding glacier.

**Keywords:** alpine deglaciation; demise of a small glacier; supraglacial debris; post-glacial landscape evolution

## 1. Introduction

Global warming is causing significant changes to alpine landscapes, with the most notable being the accelerating loss of glacier mass [1,2]. In the Austrian Alps, this has led to a 44% reduction in glacier area since the Little Ice Age (LIA) until 2004–2012 [3] and this trend is projected to continue in the future [4]. Deglaciation results in the emergence of proglacial landscapes and steep rock faces, which are characterized by periglacial and paraglacial processes. Periglacial environments are characterized by freeze–thaw processes and the presence of permafrost (see [5]), while paraglacial environments are directly conditioned by former glaciation and are dominated by sediment transport and deposition (see [6]). As these landscapes are in an unstable condition, they exhibit high geomorphic activity due to paraglacial processes (e.g., [6–9]). Concurrently, warming permafrost (e.g., [10,11]) can contribute to the destabilization of rock faces [12–15]. This may affect landscape development by increasing the input of debris to the glacier from remobilized lateral moraine deposits (e.g., [16]) or gravitational processes originating from the steep walls of the glacier catchment, such as snow avalanches (e.g., [17]), rockfalls, or rock avalanches (e.g., [18–20]). Globally, 4.4% of the glacier area is covered by debris [21], with a mean debris cover of 22.8% for the Eastern Alps in 2015, and an increasing trend [22]. This is attributed to englacial transport and increased melt-out of debris in the ablation

zone due to negative mass balances and higher ablation rates [23,24]. In comparison, when deposited in the ablation zone, the debris remains on the surface of the glacier and forms a supraglacial debris cover without being previously incorporated into the glacier and transported englacially. The increase in equilibrium line altitude (ELA) in recent decades [25] has expanded the ablation zone of glaciers, making the input of debris and the resulting supraglacial debris cover increasingly important in the future. This is particularly the case when glaciers are below the ELA and debris from steep glacier headwalls is deposited directly on the ablation zone. By the end of the century, the ELA is projected to surpass the elevation of most glaciers in the European Alps that have survived until then [26]. When a critical debris thickness is exceeded, the underlying glacial ice is insulated from atmospheric heat due to the low thermal conductivity of the debris layer, resulting in a decrease in ablation rates [27]. Therefore, depending on debris thickness and external forcing, glacier ice can remain under a debris layer long after glaciation and, in some cases, form prominent periglacial landforms (e.g., [28–30]). Although the origin of rock glaciers remains controversial (see [31]), recent case studies have even suggested the transition from debris-covered glaciers to rock glaciers over the last decades [32–36] and this process has been modeled [37].

There is a scarcity of studies that have examined the geomorphological evolution of large-scale rockfalls from the headwall of small, retreating glaciers. However, as previously discussed, we postulate that this process will become increasingly significant and may impact the appearance and development of formerly glaciated landscapes in the future. To address this gap in knowledge, the aim of this study is to present a case study that examines the geomorphological development of a rockfall on a small glacier in the Horlachtal, Stubai Alps, Austria. We also discuss its potential future evolution and the broader implications of this process for future landscapes. The investigation is based on various remote sensing data, including photogrammetrically and airborne laser scanning (ALS)-derived digital elevation models (DEMs), orthophotos, and satellite data. Although the debris-covered portion of the glacier created by the rockfall is not yet an independent landform, for the purposes of this study, we refer to it as a landform.

## 2. Materials and Methods

### 2.1. Study Area

The study area is located in the Zwieselbachtal, a north–south trending tributary valley of the Horlachtal, which is situated in the Central Eastern Alps and is part of the Stubai Alps mountain range (Figure 1a). The Horlachtal stretches over elevations of 1557 m to 3340 m and contains four recent glaciers [38] and 40 intact rock glaciers [39]. The meteorological station Horlachalm, located within the catchment at an elevation of 1910 m and operated by the Tyrolean Hydropower Company TIWAG, measured a mean annual precipitation total of 820 mm and a mean annual air temperature of 3.1 °C between 1991 and 2020. Geologically, the Horlachtal is part of the Ötztal Massif and is characterized by gneisses and mica schists dipping in an east–west direction parallel to the main valley. The north-facing Zwieselbachferner is located at the head of the Zwieselbachtal at an elevation range of 2667 m to 2943 m in 2022 (Figure 1b). The glacier, which is rather small and heavily covered with debris over large areas, currently covers an area of 0.26 km$^2$, while during the Little Ice Age (LIA) it had an area of 1.89 km$^2$ and was connected to today's Zwieselbachferner West [40]. The headwall of the glacier has an average slope of 48° and is composed of migmatite, migmatitic biotite-rich granites, and fine-grained biotite schist [41]. During the airborne laser scanning campaign, which was carried out by the Chair of Physical Geography of the University of Eichstätt-Ingolstadt in 2022 as part of the SEHAG ("Sensitivity of high alpine geosystems to climate change since 1850") project, a debris-covered part of the glacier was discovered on the Zwieselbachferner, which is clearly distinguishable from the remaining part of the glacier (Figure 1c).
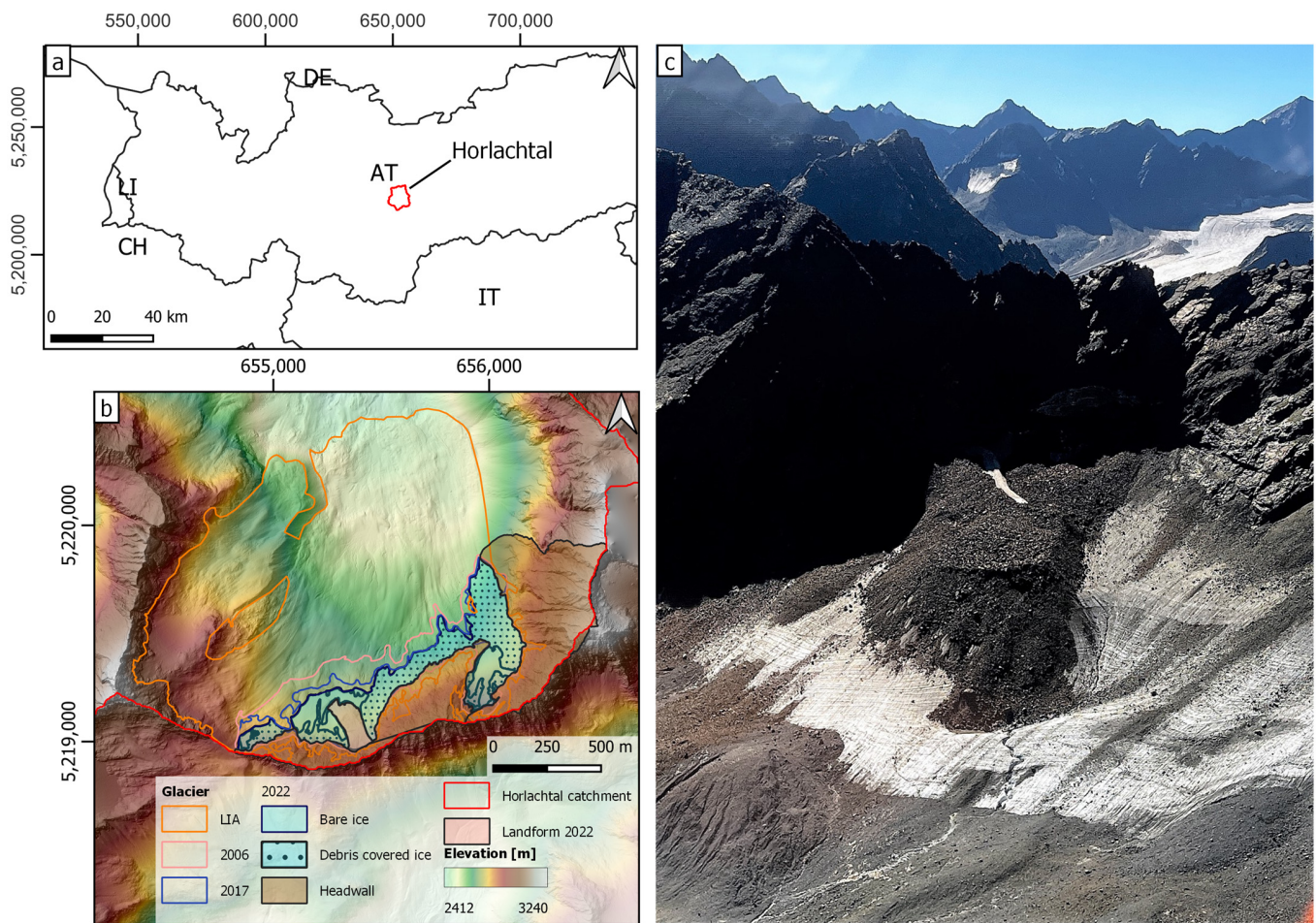
**Figure 1.** (**a**) Location of the Horlachtal in Austria and surrounding countries. The coordinates in this figure, as well as in all following figures of this study, are ETRS89/UTM zone 32N coordinates (EPSG: 25832). (**b**) Overview map of the study area in Zwieselbachtal. The mapping of glacier extents, glacier headwall, and landform is described in more detail in Section 2.3. The LIA glacier extent is taken from the Austrian Glacier Inventories [40]. (**c**) Aerial photo of the landform, whose development is being studied, taken during the ALS campaign on 03 August 2022.

## 2.2. Data and Data Pre-Processing

To reconstruct the formation of the landform and characterize its development, several remote sensing data sets were used. The data sets, their use, and their pre-processing for further analyses are described in the following. The uncertainties and shortcomings of the data and methods are discussed in Section 4.1.

### 2.2.1. Digital Elevation Models

Both photogrammetrically and ALS-derived DEMs (see Table 1) and their derivatives (hillshade and slope rasters) were used for mapping, while volume and surface elevation change calculations were performed based on DEMs of Differences (DoDs).

For 1973, the pre-rockfall DEM, a total of 91 aerial images, scanned with 12 µm, were obtained from the surveying department of the federate state Tyrol (www.tirol.gv.at, accessed on 20 January 2023). The images were acquired with a Wild camera equipped with a 210 mm lens. The images were oriented using an aerial triangulation [42] in the Software Trimble Inpho 9.2 using 62 manually picked ground control points (GCPs) with an accuracy of 0.2 pixels. The GCP coordinates were derived from a recent orthophoto and elevation model. After this image orientation, surface points (mean point density 1.8 pts/m$^2$) were derived using feature-based matching to create a surface model and an orthophoto mosaic.

**Table 1.** Information on the DEMs used in this study.

| Date | Data Type | Source | Point Density (pt/m$^2$) | Raster Resolution (m) |
|---|---|---|---|---|
| 6 August 1973 | Photogrammetric point cloud | Images: State Tyrol; own processing | 1.8 | 1 |
| 6–7 September 2006 | ALS raster | State Tyrol | - | 1 |
| 19, 31 July 2017 | ALS raster | State Tyrol | - | 1 |
| 22 September 2021 | ALS point cloud | Own acquisition/ processing | 13.7 | 1 |
| 4 August 2022 | ALS point cloud | Own acquisition/ processing | 21.6 | 1 |

The DEM from 2006 and 2017 were provided by the state of Tyrol. These ALS-derived datasets are available as gridded DEMs at a resolution of 1 m × 1 m.

The ALS data from 2021 and 2022 were recorded during two field campaigns of the University of Eichstätt-Ingolstadt on 22 September 2021 and 4 August 2022 using a Riegl VUX 1LR integrated into a Riegl VP-1 HeliCopterPod (see https://riegl.com accessed on 20 January 2023) mounted on a helicopter. The processing of the raw data included the correction of the trajectory using a virtual reference station calculated by real-time positioning Austria—EPOSA (eposa.at). Individual stripes were georeferenced with parameters optimized by automatic strip adjustment [43], which is implemented in the point cloud processing software OPALS [44]. Outlier detection and ground point classification were performed using the LIS Pro 3D extension of Laserdata [45] of the GIS software SAGA [46]. Following point cloud processing, the point clouds were gridded with a resolution of 1 m × 1 m.

As the datasets of 2006 and 2017 are only provided as gridded DEMs and not point clouds, we used the grid-based approach for iterative co-registration of DEMs proposed by Nuth and Kääb [47], implemented in the Python package pybob [48] for fine registration of the DEMs. Based on the orthophoto and initial DoDs (DoDs without prior fine registration), stable bedrock sections and stable areas in the glacier forefield around the study area were mapped and used for the fine registration of all datasets to the DEM 2017, which served as the reference dataset.

For all calculations of surface elevation change and volume calculations based on DoDs, an uncertainty analysis according to Anderson [49] was carried out. For all periods, a 670 m$^2$ stable rock surface with similar exposure and slope inclination as the investigated areas was taken as a basis for this analysis (for a more detailed description of the uncertainty analysis, see Anderson [49] and Fleischer et al. [50]).

### 2.2.2. Orthophotos

In addition to mapping the snow patches on the landform and the debris cover of the Zwieselbachferner (Section 2.3), orthophotos were used to determine the flow velocities of the landform (Section 2.7). Table 2 lists all the orthophotos used. Orthophotos with a resolution of 0.2 m were obtained from the Office of the Tyrolean Government, Department of Geoinformation/Tyrol, Austria. The software Agisoft Metashape Professional 1.7.2 was utilized in a standard structure from motion, multi-view stereo (SfM-MVS) workflow, to calculate an orthophoto of 2022 using 39 photos from a nadir camera (Sony α7R + Zeiss Loxia 2.4/25 mm) which was mounted on the helicopter during the 2022 ALS campaign. After aligning the photos, they were georeferenced by selecting 10 GCPs in and around the landform on the DEM of 2022. The simultaneous acquisition of the images and the ALS data justifies the determination of GCPs even in non-stable areas. Before the creation of the dense point cloud, the DEM calculation, and the creation of the orthophoto, a bundle adjustment was carried out. The resulting orthophoto was resampled to a resolution of 0.2 m to match the resolution of the orthophotos from 2003 to 2018. To align the orthophotos

and thus improve the spatial accuracy of the results, they were manually co-registered with the 2015 orthophoto (see [51]).

**Table 2.** Information on the orthophotos used in this study.

| Date | Type | Source | GSD * [m] |
|---|---|---|---|
| 4 August 1973 | Photogrammetric orthophoto | Images: State Tyrol; own processing | 0.2 |
| 4 September 2003 | Orthophoto | State Tyrol | 0.2 |
| 8 September 2009 | Orthophoto | State Tyrol | 0.2 |
| 27 August 2015 | Orthophoto | State Tyrol | 0.2 |
| 27 September 2018 | Orthophoto | State Tyrol | 0.2 |
| 4 August 2022 | Photogrammetric orthophoto | Own acquisition/ processing | 0.03 |

* Ground sampling distance.

### 2.2.3. Satellite Images

To determine the initial rockfall event that formed the landform, Landsat 5 and 7 satellite images (https://earthexplorer.usgs.gov/ accessed on 12 December 2022) from 2000–2006 were analyzed in addition to available orthophotos. The temporal delineation was possible because the occurrence of the initial rockfall could be narrowed down in advance using Google Earth images (https://earth.google.com accessed on 5 December 2022) and the available ALS data and orthophotos. Furthermore, freely available satellite images from Sentinel 2 and Landsat 5, 7, and 8 satellites between July and October were used to visually determine whether the glacier was below or above the ELA in the respective year (Table S1 and Figure S1). A distinction was made between the slightly higher part (eastern part) and the rest of the glacier (western part), where the landform is located.

### 2.3. Glacier and Landform Mapping

Manual mapping of debris-covered glacier ice can be challenging and is prone to error even on high-resolution data [52]. However, Abermann et al. [53] have demonstrated the potential of multi-temporal, high-resolution DEMs for mapping glaciers and debris-covered glaciers. Adopting this method, which has been used for mountain regions [54] as well as individual glaciers [55], we use DoDs to map the extent of the Zwieselbachferner. In this way, the glacier outlines of the years 2006 and 2017 can be determined. To map the outline of the glacier in 2022, a DoD was generated from the DEMs 2021 and 2022. The resulting 2021 glacier outline was corrected by visual inspection of the 2022 hillshade to obtain the 2022 outline. In addition, the bare ice was mapped on the available orthophotos. Due to the mapping approach of the glacier outlines, it is not possible to determine the proportion of the debris-covered area to the total glacier area, because apart from 2022 there are no glacier outlines that temporally match the mapping of the bare ice on the orthophotos.

The mapping of the Landform was carried out both on hillshades derived from DEMs and on orthophotos. Snow patches that were present at the time when the respective datasets were recorded were also mapped. All mapping was completed by one operator, as this increases the consistency of the results [56]. Subsequently, the co-authors reviewed the mapping.

### 2.4. Characterization of Rockfalls

In a first step, the rockfall detachment areas of the periods 1973–2006, 2006–2017, and 2017–2022 were mapped in the headwall based on the respective DoDs. The DEM 1973 was used as the pre-initial rockfall DEM, as it provided the best data quality of the associated aerial photographs. Other possible data sets for the pre-rockfall DEM would have been the aerial photographs from 1997 or 2003 (Federal Office of Metrology and Surveying

(BEV) but were discarded due to quality issues. While the area of the glacier headwall is heavily shadowed in the 1997 aerial photos, the 2003 data set shows snow in this area. Both snow and shadows are disadvantageous for photogrammetric processing and DEM creation. Visual comparisons of the 2003 and 1973 orthophotos indicate that no major rockfalls occurred in the glacier headwall above the landform during this period. To avoid misunderstandings, we use 2003–2006 for this period in the following text and note that volume calculations of this period were calculated based on the DoD 1973–2006.

After mapping the rockfall detachment areas in the headwall above the glacier, their volumes were calculated for each area based on the DoDs. Due to the time difference between the single remote sensing data acquisitions, it is not possible to say with certainty whether the volume changes in the individual areas occurred in one or in several single rockfall events.

To represent the thermal regime in the rock face and to draw links between rockfall activity and the presence of permafrost, permafrost modeling based on Kenner et al. [57] was carried out. This model uses a linear regression with the explanatory variables potential incoming solar radiation (PISR) and elevation to predict borehole temperatures and therefore model the mean annual ground temperature (MAGT) and thus permafrost occurrence. This model was developed in the Swiss Alps and, in the form adopted in this study, is valid for ice-poor permafrost in rockwalls.

### 2.5. Estimation of Initial Debris Thickness

To estimate the spatial distribution of the initial rockfall debris thickness, cross-sections with a spacing of 10 m over the DEM from 2006 were analyzed. Additionally, the landform mapped in 2006 was clipped from the DEM 2006 and the resulting gap was closed using bilinear interpolation to reconstruct the glacier surface [58,59] under the debris layer. To obtain a spatially distributed debris thickness layer, the actual surface was subtracted from the interpolated surface.

### 2.6. Measurement of Surface Elevation Changes and Estimation of Ice Thickness Development

Because spatially high-resolution surface elevation changes in the glacier are available for the periods 2006–2017 and 2017–2022 from DoDs, we wanted to illustrate this effect on ice thickness to estimate its past and future development. As a basis for this, we use ice thickness data produced by Helfricht et al. [60]. They used in situ ice thickness measurements of glaciers in the Austrian Alps and observed glacier geometries to calibrate an established ice thickness model [61] and derive an ice thickness dataset for all glaciers in the Austrian Alps. This data set was subtracted by the surface elevation changes in each period. The results were clipped by the mapped glacier outlines to derive the ice thickness for the years 2017 and 2022. Assuming a consistent annual rate of surface elevation change, derived from the 2017–2022 DoD, we estimate the future evolution of ice thickness.

### 2.7. Measurement of the Surface Flow Velocities

To determine the flow velocities of the landform, image correlation, and manual feature tracking methods were applied using orthophotos from 2009, 2015, 2018, and 2022, with snow-covered areas excluded. Image correlations were calculated utilizing the IMCORR algorithm [62] implemented in SAGA GIS (configuration: search chip size: 128 × 128; reference chip size: 64 × 64; grid spacing: 5). This method generates vectors representing the flow direction and distance between two images (e.g., [51,63,64]). These were cleaned manually, and a level of detection (LoD) was determined according to the approach of Fey and Krainer [63]. Additionally, 22 blocks distributed over the landform were tracked manually. The presence of thin snow cover on the surrounding glacier in the 2009 and 2018 orthophotos hampered a similar analysis of possible glacier movement.

## 3. Results

### 3.1. Evolution of the Zwieselbachferner

At the maximum extent of the LIA, the Zwieselbachferner had an area of 1.87 km$^2$ and, following the alpine-wide trend [3], had melted to an area of 0.42 km$^2$ by 2006, creating a typical proglacial landscape see [8]. The glacier area is reduced by 27% to 0.31 km$^2$ by 2017 and by another 14% to 0.26 km$^2$ by 2022. Although the majority of the glacier is already covered by debris in 2006, this area increased to 77% of the total glacier area by 2022 (Figure 1b). The analysis of satellite imagery from 2004 to 2022 shows that the ELA in the western part, where the landform is located, is situated above the glacier in 50% of the years, while this is the case for the eastern part in 20%. These data are based on cloud-free and snow-free images, as no such images were available between 2007–2008 and 2012–2014. As the glacier is below the ELA in certain years, the melting of englacial debris in the upper zone of the glacier occurs. Moreover, debris transported from the headwall accumulates, as evidenced by the results of clean ice mapping on the orthophotos, which show an increase in debris coverage on the upper parts of the glacier between 2009 and 2022. The mean surface elevation change in the glacier slightly increases, despite the increase in debris cover, with a rate of −0.76 m/year ± 0.01 m/year from 2006 to 2017 and −0.83 m/year ± 0.01 m/year from 2017 to 2022. This results in a total volume loss of −315,335 m$^3$/year ± 4506 m$^3$/year and −255,666 m$^3$/year ± 1860 m$^3$/year, respectively.

### 3.2. Evolution of the Landform

The analysis of the LANDSAT data indicates that the initial rockfall on the Zwieselbachferner occurred between 4 September 2003 and 18 September 2004. For this rockfall, a volume of 19,267 m$^3$ ± 204 m$^3$ can be determined. Regarding the estimated debris thickness of the initial rockfall deposition, we refrain from giving absolute values but give a continuous scale from thin to thick due to the methodology. Visual observation of the hillshades and orthophotos suggests that the minimum thicknesses (thin) are a few decimeters, while analysis of the profiles (Figure S2) suggests that the maximum thickness (thick) is several meters. In the upper part of the landform, the more complex topography of the glacier even led to negative values, which were classified as thin debris thickness, confirmed by the hillshade of the DEM of 2006 and the orthophoto of 2009 (see Section 4.1. for more detail). The debris thicknesses estimation after the initial rockfall indicates that the greatest thickness occurs at the down-glacier part of the landform, decreasing towards the headwall of the glacier (Figure 2a). The distance from the initial rockfall detachment area to the front of the mapped landform in 2006 is up to 240 m, which indicates a long run-out length of the initial rockfall on the glacier (c.f. [15]). The locations of major rockfalls between 2003 and 2022 are illustrated in Figure 2. These include two large rockfalls between 2003 and 2006, with volumes of 2248 m$^3$ ± 36 m$^3$ and 2009 m$^3$ ± 27 m$^3$. Between 2006 and 2017, there were eight additional rockfalls, ranging in volume from 70 m$^3$ ± 6 m$^3$ to 4250 m$^3$ ± 121 m$^3$. In the period from 2017 to 2022, three more rockfalls were identified, with volumes between 99 m$^3$ ± 2 m$^3$ and 1305 m$^3$ ± 16 m$^3$. It is not possible to determine the deposition area of the rockfalls following the initial event based on the DoDs due to the changing surface elevation of the glacier. However, a visual comparison of the available orthophotos indicates that the rockfalls had shorter run-out lengths and were mostly deposited on the upper part of the landform. Some rockfall detachment areas (Event IDs: 01_03, 02_01, 02_02, 02_03, 03_02) deposited debris partly on the glacier next to the landform, resulting in an elongated debris cover in that area due to longer run-out lengths on the ice.

For the entire area of the glacier headwall, MAGT was below 0 °C and thus permafrost was modeled (Figure 2). In the area of the headwall above the landform, which is geologically composed of migmatites [41], a minimum MAGT of −3.34 °C was calculated. However, in this area, the headwall is built up by a relatively narrow ridge, on whose southeast-facing side we derived MAGT temperatures between 0 °C and 1 °C in some areas.

The thick debris cover on the landform reduces melting rates, as evidenced by the lower surface elevation changes. The mean surface elevation changes were −0.23 m/year ±

0.01 m/year and −0.29 m/year ± 0.01 m/year between 2006–2017 and 2017–2022, respectively. Comparison of the surface elevation change rates in an area of 50 m around the landform shows a reduction by a factor of four and five, respectively, in the two periods. When only bare ice around the landform is considered, the reduction factors increase to six and seven, respectively. This leads to the formation and steepening of the sides and front of the landform (Figure 3).
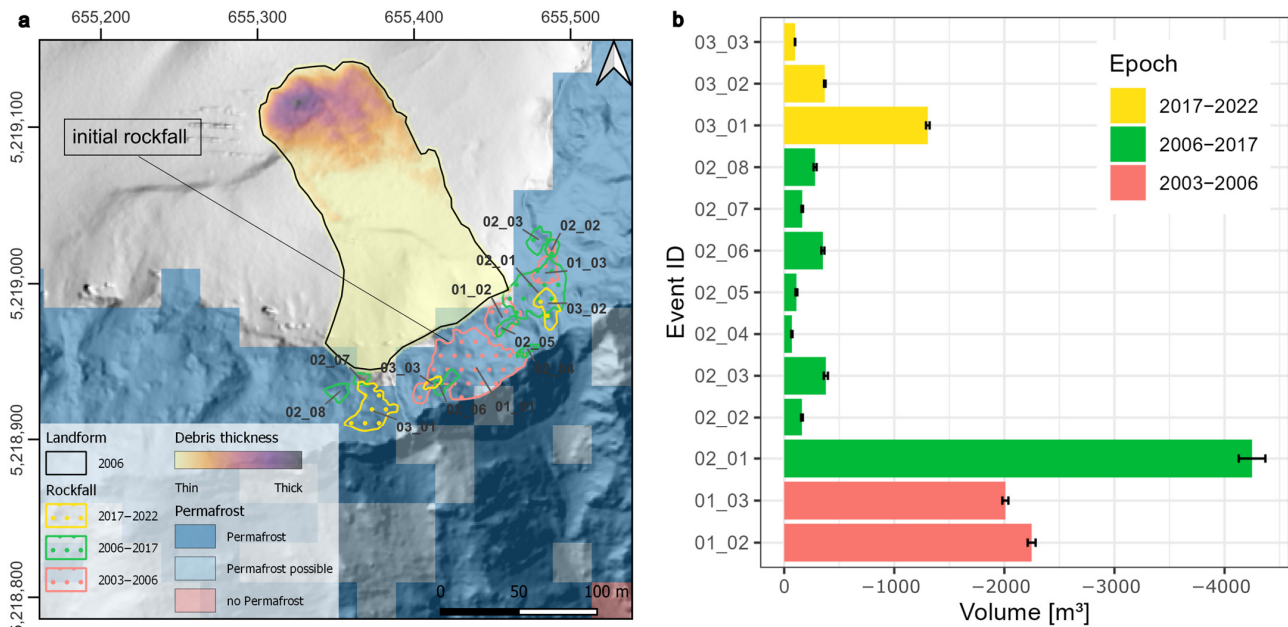


**Figure 2.** (**a**) Rockfall detachment areas, which are mapped based on DoDs, modeled permafrost occurrence following the approach of Kenner et al. [57] and estimated debris thickness after the initial rockfall. (**b**) Volume of rockfalls calculated based on DoDs. The initial rockfall, which has a volume of 19,267 m$^3$ ± 204 m$^3$, is not plotted.
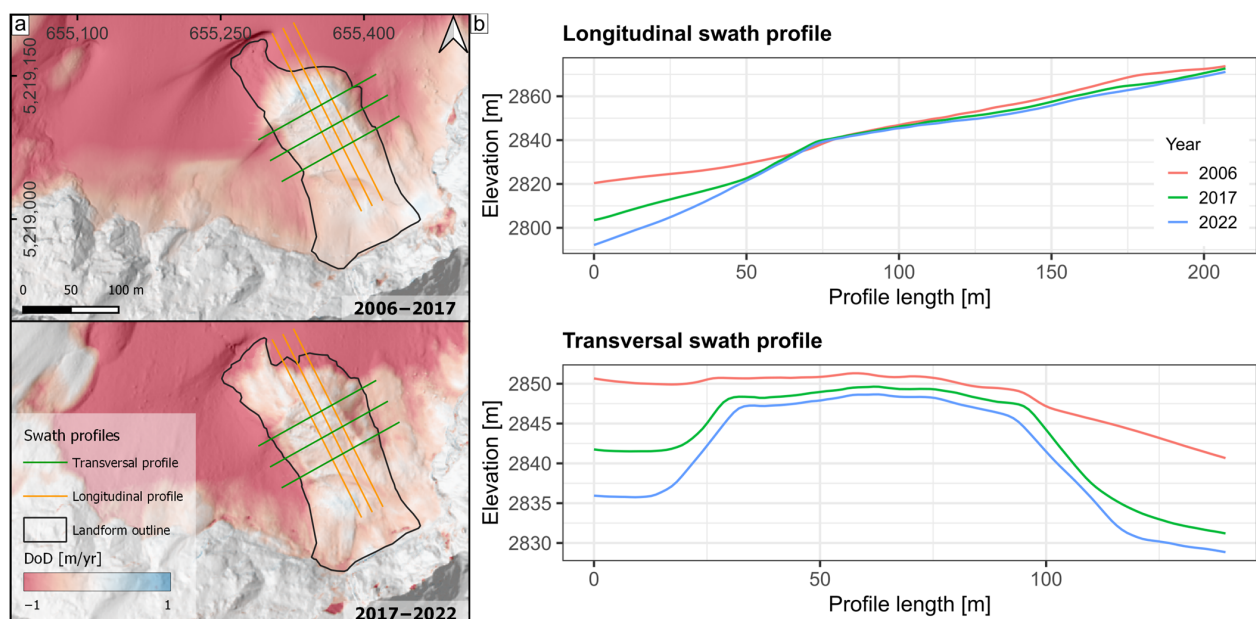


**Figure 3.** (**a**) Mean annual surface elevation change in the landform and the surrounding glacier. (**b**) Mean elevation in the transverse and longitudinal swath profiles (50 m), represents the mean change in the shape of the landform. The locations of the profiles are shown in (**a**).

The reduced surface elevation changes on the landform lead, in consequence, to more ice being preserved underneath (Figure 4). As can be seen on the maps of ice thickness development in Figure 4, the glacier around the landform is melting and is clearly losing thickness. The mean ice thickness in the landform area decreases only slightly from 23.5 m to 21.81 m between 2006 and 2022, while the maximum ice thickness remains constant at about 40 m over the same period.
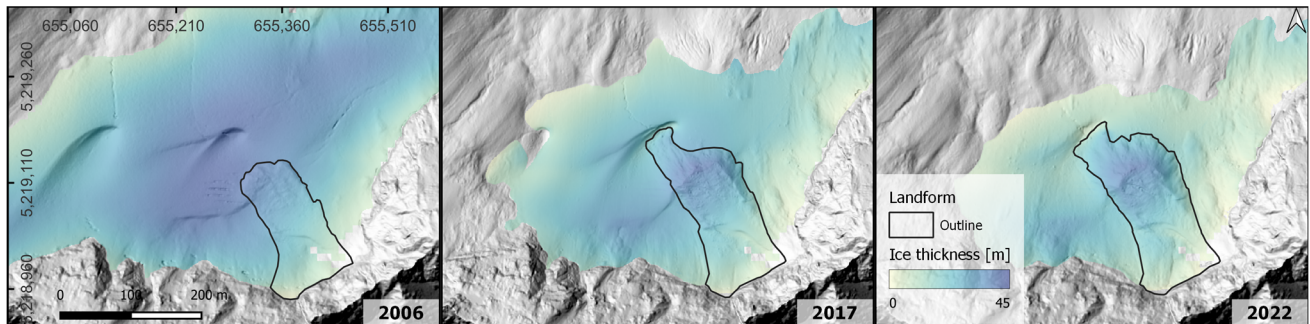


**Figure 4.** Development of ice thickness of the Zwieselbachferner. The initial ice thickness (2006) is modeled by Helfricht et al. [65], and the further development of ice thickness is derived by subtracting the respective DoDs from this data (for a more detailed description of the approach see Sections 2.6 and 4.1).

The development of the surface flow velocity of the landform was investigated using both image correlation and manual mapping of orthophotos. The results of both methods were found to be consistent and showed a directional homogeneity in flow velocity across all periods (Figure 5). The LoD of flow velocities were determined to be 0.035 m/year (2009–2015), 0.071 m/year (2015–2018), and 0.063 m/year (2018–2022). The mean value of the flow velocity decreased over time, from 0.77 m/year (2009–2015) to 0.61 m/year (2015–2018) and finally to 0.41 m/year (2018–2022). The flow velocity maps show an inhomogeneous deceleration towards the current rate in the 2018–2022 period with little spatial variability.
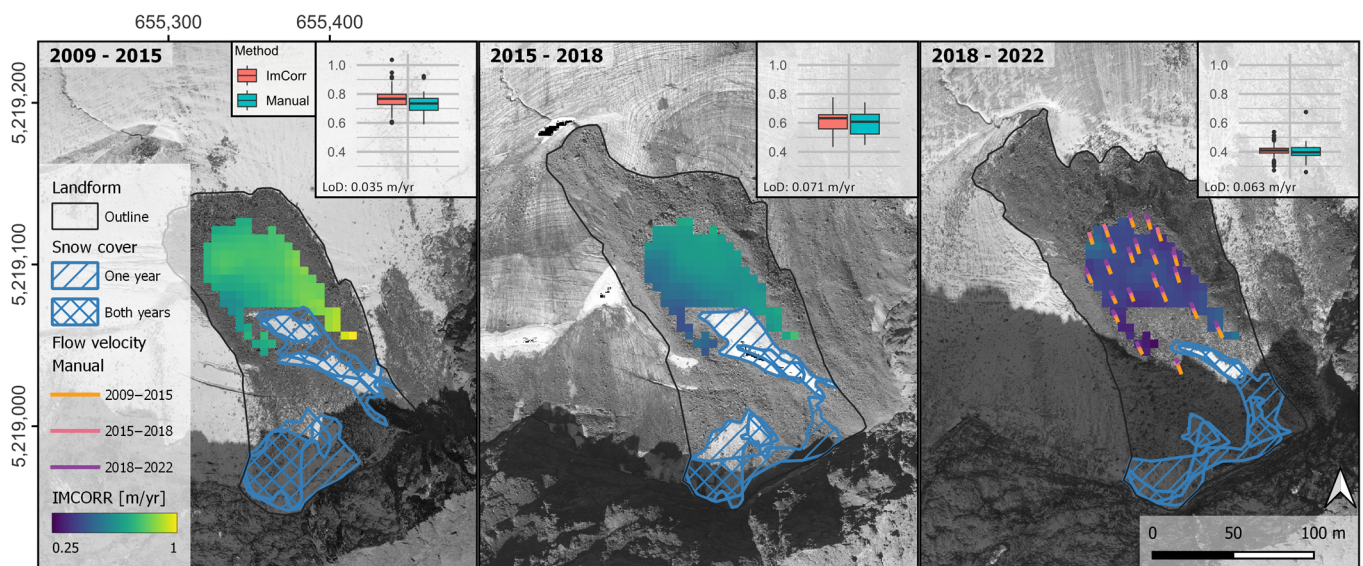


**Figure 5.** Flow velocity in different periods derived by manual mapping and image correlation (IMCORR). The landform outline and the orthophoto depict the first year of the respective period. In the upper-right corner of the individual maps, flow velocities of the period are displayed as boxplots with the unit m/year. The results of the manual mapping are shown for all periods in the map of the period 2018–2022.

## 4. Discussion

### 4.1. Methodological Limitations

To estimate the spatial distribution of debris thickness following the initial rockfall, we reconstructed the glacier surface from the DEM of 2006. While bilinear interpolation is generally considered a reliable method for dealing with DEM voids for glacier applications [58], it is important to note its limitations for our application. This method is not capable of reconstructing the actual glacier surface for sections with complex topography, which led to negative values in the upper part of the landform when estimating debris thickness. Additionally, the lack of an elevation model shortly after the initial rockfall results in an overestimation of the debris cover due to differences in surface elevation changes between the landform and surrounding glaciers.

It is important to note that the differences in surface elevation changes between landforms and surrounding glaciers are primarily attributed to variations in melt rates of the underlying and surrounding glacier ice, caused by the insulation effect of the debris mass [27]. However, other factors such as surface elevation changes resulting from downslope movement, debris redistribution, and input from headwall avalanches and debris, as well as compaction of debris and ice aggregation, can also contribute to an underestimation or overestimation of the actual melt rate. The same considerations apply to the calculation of ice thickness development, as surface elevation changes were assumed to reflect melt rates. Additionally, model inaccuracies of 25–30% [65] should be taken into account when estimating future ice thicknesses under the assumption of constant melt rates. It is also important to consider that this assumption may not be accurate due to potential future changes in meteorological forcing and debris cover extent and thickness.

### 4.2. Similar Landforms

Kellerer-Prikelbauer and Kaufmann [30] studied the deglaciation of two neighboring cirques in the Schober Mountains, Austria, which no longer contain glaciers. They observed "small scale tongue-shaped landforms" (STLs) beneath the cirque headwalls, similar to those described by Gómez et al. [29]. These STLs have lengths of 38–125 m, front heights of 1–6 m, widths of 13–34 m, and average slopes of 24–34 degrees. In 2022, the landform described here was found to be larger in size and the front height was significantly greater, around 30 m. The authors used electrical resistivity tomography and ground surface temperature measurements to detect permafrost and massive ice in the STLs. The debris thickness of the STLs is 40–70 cm, significantly lower than the debris thickness of up to several meters estimated for the terminal area of the landform. They also found consistent horizontal movement velocities of 1 m/year between 1997 and 2002 and vertical subsidence of the STLs. The formation of these landforms is explained by paraglacial slope processes, which deposited debris on the former glaciers [30].

Beyond the previously mentioned glaciogenic periglacial landforms, additional rockfalls have been observed on glaciers, which could contribute to the creation of analogous landforms. Although no systematic analysis was conducted in the present study, Figure S3 depicts several examples from the Eastern Alps.

### 4.3. Interpretation of Landform Development

Although a comparison of the orthophoto from 1973 and 2003, which is partially obscured by snow, did not reveal a large rockfall in the headwall above the landform. Rockfalls, both large and small, occurred in the years following the initial event, which is thought to have taken place between 4 September 2003 and 18 September 2004. This may indicate a change in the system and explain the high rockfall rates in the decades following deglaciation [9]. Additionally, warming permafrost, particularly an increase in the active layer thickness [10,11], may also play a role in destabilizing the rock face and leading to high-magnitude rockfalls and a higher rockfall frequency [12,13,66]. The exact year of the first major rockfall could not be determined, but a heat wave in the summer of 2003 may have been a contributing factor [67]. Additionally, we assume that the area above the

landform is characterized by weaknesses in the lithology, as the frequency and magnitude of rockfalls in this area are significantly higher than in other areas of the headwall. This is evident from the visual analysis of the DoDs.

The greatly reduced surface elevation changes observed in the area of the rockfall deposits on the glacier are attributed to reduced melt rates of the underlying glacier due to the insulation effect of the thick debris cover. This results in a longer preservation of the ice, leading to comparatively faster melting of the surrounding glacier and the formation of a steep flank and front of the landform. Due to the lateral melting of the ice body, the debris lying on the top edges lose its support. This leads to smaller-scale mass movements and consequently to the covering of the flanks with debris, resulting in an increase in the area of the landform (Figure 3; orthophotos and outlines in Figure 5). Insolating the flanks with debris causes reduced melt rates and can be described as a negative feedback loop.

Unfortunately, we were unable to determine the flow velocity of the surrounding glacier using the methods employed to measure the surface flow velocity of the landform. As a result, we are unable to provide a proportion of the surface flow velocity of the landform compared to glacier movement. However, it is likely that the measured surface flow velocity is a combination of glacier creep, sliding of the debris mass on the debris–glacier interface, and deformation processes within the debris mass.

### 4.4. Future Development of the Landform

Our aim in the following discussion is to examine processes that may impact the future development and appearance of the landform. Due to the challenge of extrapolating external forcing, processes, and process rates, they should be viewed as possibilities rather than deterministic predictions. The manifestation and the interaction of these processes, including the melt rate of the ice core, development of surface morphology, material supply, and flow velocity, will govern the preservation and evolution of the landform in the coming years or decades.

### 4.4.1. Ice Thickness

Based on constant changes in surface elevation and past ice thickness developments, it is likely that the glacier at the front of the landform will have melted by 2032. By 2042, most of the surrounding glaciers will have melted, leaving only debris-covered dead ice at the base of the headwall (Figure 6). However, it is important to note that the timing of these developments is approximate and subject to change. Despite this, it can be inferred that the landform will likely outlast the surrounding glacier and can then be considered an independent landform. The complete melting of the glacier marks the transition of the system from a glacial to a periglacial [5] one.

### 4.4.2. Surface Morphology

If permafrost conditions prevail, the ice beneath the debris layer may melt if it is thinner than the active layer [31]. The low standard deviations in surface elevation change of 0.11 m/year and 0.16 m/year, respectively, have resulted in a relatively uniform landform evolution since 2006 (see Figure 3). However, the melt-out of englacial debris and the redistribution of debris by gravitational processes could potentially increase debris thickness and alter its spatial variability [23,68]. Consequently, this would lead to the development of incoherent surface morphology, due to variable melt rates, if the spatial distribution of debris thickness exhibits small-scale variability. This was observed for debris-covered glaciers by Mölg et al. [69] and Westoby et al. [70].
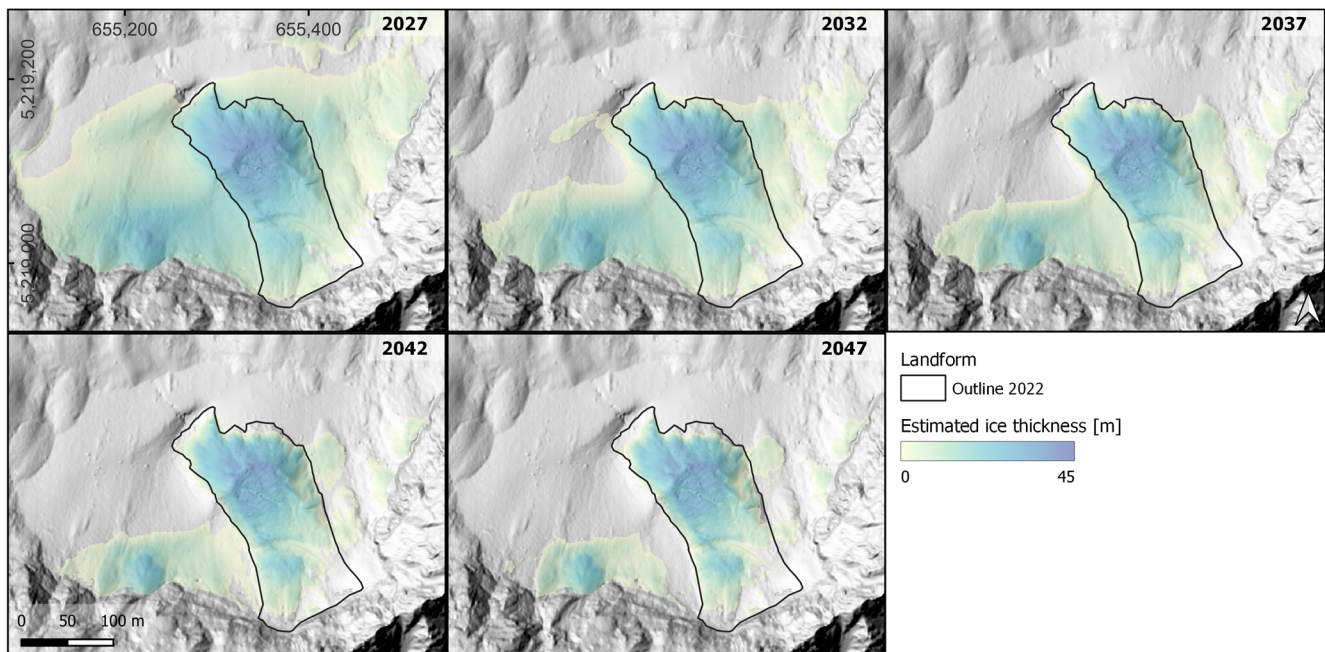
**Figure 6.** Estimated future development of ice thickness and glacier extent in five-year steps assuming constant surface elevation changes regarding the period 2017–2022. The base map for all years is the hillshade of the DEM from 2022. Additional processes, including the redistribution of debris, the development of surface morphology, and flow movement, along with debris and avalanche input from the headwall, will alter the extent and appearance of the landform compared to its current state in 2022. It should be noted that these changes are not accounted for in this figure.

### 4.4.3. Permafrost Conditions

Permafrost formation may occur after deglaciation of an area [71–73]. Due to the lack of in situ measurements, (e.g., MAGT or bottom temperature of snow cover measurements) it is difficult to prove permafrost, which is defined in the classic sense as ground that has temperatures below or at 0 °C for two consecutive years [74]. Glacier ice is often excluded (e.g., [75]), while old debris-covered glacier ice was later often included in the permafrost definition (e.g., [76]). Following the latter definition, the landform after deglaciation of the surrounding Zwieselbachferner would be considered permafrost. At least in the upper part of the landform, permafrost in the classical sense can be assumed under the perennial snow patches (see Figure 5). They favor the development of negative ground temperatures as temperatures cannot rise above zero during the summer while temperatures drop far below zero during the winter and therefore contribute to the accumulation of frozen material [77].

### 4.4.4. Sediment and Ice Supply

Our observations show that the rate of rockwall retreat at −43 mm/year ± 6 mm/year in 2017–2022 and −33 ± 11 mm/year in 2006–2017 is significantly higher compared to alpine rockwall erosion in general (see [78] and references within). It is worth noting that a significant part of the rockwall retreat rate is caused by large rockfalls, the future development of which cannot be predicted with the available data. In addition, the time period from 2006 to 2022 is not extensive enough to confidentially estimate sediment source rates in general. Nonetheless, the occurrence of 13 rockfalls, with volumes ranging from $67 \text{ m}^3 \pm 6 \text{ m}^3$ to $4250 \text{ m}^3 \pm 121 \text{ m}^3$ between 2003 and 2022 (see Figure 2) suggests that rockfalls in this headwall area are expected to continue in the future, contributing debris to the upper region of the landform. While the ELA is projected to increase in the future [26], in the case of the Zwieselbachferner, it is anticipated to be below the glacier limit in some of the years to come. This was observed in 50% of the years during the study period, and no distinct trend was observed. In years when the ELA was above the glacier, snow

patches were identified in the upper section of the landform, some of which were perennial (see Figure 5). Given the existence of snow in the upper part of the landform, combined with anticipated rockfall activity in the area, snow may be preserved by debris-induced accumulation (see [79]).

### 4.4.5. Flow Velocity

The measured surface flow velocities of 0.41 m/year in the recent past (2017–2022) do not provide any conclusive information on the future flow of the landform once the surrounding glacier has melted. However, other similar landforms that also exhibit an ice core and similar slopes have had surface flow velocities measured after deglaciation [30]. This is not surprising given that even completely buried glacier ice will continue to flow if the shear stress is high enough to exceed the yield stress of the ice body [31]. Additionally, Azizi and Whalley [80] have modeled the flow of similar landforms that consists of an ice core and a debris layer. Assuming this structure of the landform, the current and future surface flow velocity is primarily the result of basal sliding and sliding of the debris layer on the debris–glacier interface [81].

## 5. Conclusions

In this study, we examined the morphological evolution of a rockfall onto a small glacier below the ELA in many of the years studied. Our results suggest that the insulating effect of the debris layer on the glacier will result in a debris-covered landform with an ice core remaining in the future, even after the surrounding glacier has melted. As glaciers continue to melt rapidly, ELA rises and glacier headwalls become more unstable due to glacier melt and permafrost warming, we expect this process to occur more frequently in the future and in some cases shape the appearance of formerly glaciated landscapes. Our case study demonstrated how a rockfall-derived debris layer, estimated to be several meters in parts, greatly reduces melt rates of the underlying glacier ice. As a result of the variable melt rates of the debris cover and the surrounding glacier, a steep front and flanks form, which become progressively covered and thus insulated by debris redistribution. Furthermore, we were able to show that the underlying ice probably remains long after the surrounding glacier has melted and thus forms an independent glaciogenic periglacial landform.

In addition to the basic requirements such as the presence of a glacier below the ELA and an unstable headwall, the formation of landforms similar to the one studied in this research is also dependent on the timing, magnitude, frequency, and type of debris input. This controls the composition, thickness, width, and length of the debris, which in turn affects the area and intensity of insolation of the debris-covered glacier surface. High magnitudes of rockfall, which are crucial for the formation of these landforms, are caused by factors such as lithological weaknesses. As a result, it is likely that these phenomena mainly occur in regions where changes in permafrost interact with these lithological conditions. The persistence and future development of such landforms are also dependent on the thickness of the glacier at the time of initial deposition, as well as the melt rate of the ice core, development of surface morphology, material supply, flow velocity, and external forcing.

As glaciers continue to melt due to climate change, formerly glaciated areas will shape the landscape in the high mountains in the future. In addition to moraines, high morphodynamics due to paraglacial adjustment processes and newly formed lakes, these areas will also feature glaciogenic, periglacial landforms. A systematic analysis of debris–glacier interaction on small glaciers below the ELA, both retrospectively and prospectively, is necessary to better understand the future appearance and process dynamics of currently glaciated areas. This can be accomplished through a combination of historical maps, historical DEMs derived from historical aerial photographs, more recent ALS data, and orthophotos, in conjunction with field surveys such as measurements of MAGT and debris thickness. This would provide a better understanding of the frequency of occurrence, future

development, possible correlations with lithological conditions or relief parameters, and persistence of such glaciogenic periglacial features.

## References

1.　Hugonnet, R.; McNabb, R.; Berthier, E.; Menounos, B.; Nuth, C.; Girod, L.; Farinotti, D.; Huss, M.; Dussaillant, I.; Brun, F.; et al. Accelerated global glacier mass loss in the early twenty-first century. *Nature* **2021**, *592*, 726–731. [CrossRef] [PubMed]

2.　Zemp, M.; Huss, M.; Thibert, E.; Eckert, N.; McNabb, R.; Huber, J.; Barandun, M.; Machguth, H.; Nussbaumer, S.U.; Gärtner-Roer, I.; et al. Global glacier mass changes and their contributions to sea-level rise from 1961 to 2016. *Nature* **2019**, *568*, 382–386. [CrossRef] [PubMed]

3.　Fischer, A.; Seiser, B.; Stocker Waldhuber, M.; Mitterer, C.; Abermann, J. Tracing glacier changes in Austria from the Little Ice Age to the present using a lidar-based high-resolution glacier inventory in Austria. *Cryosphere* **2015**, *9*, 753–766. [CrossRef]

4.　Zekollari, H.; Huss, M.; Farinotti, D. Modelling the future evolution of glaciers in the European Alps under the EURO-CORDEX RCM ensemble. *Cryosphere* **2019**, *13*, 1125–1146. [CrossRef]

5.　Ballantyne, C.K. *Periglacial Geomorphology*; John Wiley & Sons Incorporated: Somerset, UK, 2017; ISBN 978-1-405-10006-9.

6.　Ballantyne, C.K. Paraglacial geomorphology. *Quat. Sci. Rev.* **2002**, *21*, 1935–2017. [CrossRef]

7.　Iturrizaga, L. Paraglacial Landscape Transformations. In *Encyclopedia of Snow, Ice and Glaciers*; Singh, V.P., Singh, P., Haritashya, U.K., Eds.; Springer: Dordrecht, The Netherlands, 2011; pp. 817–823. ISBN 978-90-481-2641-5.

8.　Heckmann, T.; Morche, D. *Geomorphology of Proglacial Systems*; Springer International Publishing: Cham, Switzerland, 2019; ISBN 978-3-319-94182-0.

9.　Hartmeyer, I.; Delleske, R.; Keuschnig, M.; Krautblatter, M.; Lang, A.; Schrott, L.; Otto, J.-C. Current glacier recession causes significant rockfall increase: The immediate paraglacial response of deglaciating cirque walls. *Earth Surf. Dynam.* **2020**, *8*, 729–751. [CrossRef]

10.　Etzelmüller, B.; Guglielmin, M.; Hauck, C.; Hilbich, C.; Hoelzle, M.; Isaksen, K.; Noetzli, J.; Oliva, M.; Ramos, M. Twenty years of European mountain permafrost dynamics—The PACE legacy. *Environ. Res. Lett.* **2020**, *15*, 104070. [CrossRef]

11.　Smith, S.L.; O'Neill, H.B.; Isaksen, K.; Noetzli, J.; Romanovsky, V.E. The changing thermal state of permafrost. *Nat. Rev. Earth Environ.* **2022**, *3*, 10–23. [CrossRef]

12.　Gruber, S.; Haeberli, W. Permafrost in steep bedrock slopes and its temperature-related destabilization following climate change. *J. Geophys. Res.* **2007**, *112*, F02S18. [CrossRef]

13. Krautblatter, M.; Funk, D.; Günzel, F.K. Why permafrost rocks become unstable: A rock-ice-mechanical model in time and space. *Earth Surf. Process. Landf.* **2013**, *38*, 876–887. [CrossRef]

14. Deline, P.; Gruber, S.; Delaloye, R.; Fischer, L.; Geertsema, M.; Giardino, M.; Hasler, A.; Kirkbride, M.; Krautblatter, M.; Magnin, F.; et al. *Ice Loss and Slope Stability in High-Mountain Regions. Snow and Ice-Related Hazards, Risks and Disasters*; Elsevier: Amsterdam, The Netherlands, 2015; pp. 521–561. ISBN 9780123948496.

15. Knoflach, B.; Tussetschläger, H.; Sailer, R.; Meißl, G.; Stötter, J. High mountain rockfall dynamics: Rockfall activity and runout assessment under the aspect of a changing cryosphere. *Geogr. Ann. Ser. A Phys. Geogr.* **2021**, *103*, 83–102. [CrossRef]

16. van Woerkom, T.; Steiner, J.F.; Kraaijenbrink, P.D.A.; Miles, E.S.; Immerzeel, W.W. Sediment supply from lateral moraines to a debris-covered glacier in the Himalaya. *Earth Surf. Dynam.* **2019**, *7*, 411–427. [CrossRef]

17. Scherler, D.; Bookhagen, B.; Strecker, M.R. Hillslope-glacier coupling: The interplay of topography and glacial dynamics in High Asia. *J. Geophys. Res.* **2011**, *116*, F02019. [CrossRef]

18. Deline, P. Change in surface debris cover on Mont Blanc massif glaciers afer the 'Little Ice Age' termination. *Holocene* **2005**, *15*, 302–309. [CrossRef]

19. Deline, P. Interactions between rock avalanches and glaciers in the Mont Blanc massif during the late Holocene. *Quat. Sci. Rev.* **2009**, *28*, 1070–1083. [CrossRef]

20. Reznichenko, N.V.; Davies, T.R.; Alexander, D.J. Effects of rock avalanches on glacier behaviour and moraine formation. *Geomorphology* **2011**, *132*, 327–338. [CrossRef]

21. Scherler, D.; Wulf, H.; Gorelick, N. Global Assessment of Supraglacial Debris-Cover Extents. *Geophys. Res. Lett.* **2018**, *45*, 11798–11805. [CrossRef]

22. Fleischer, F.; Otto, J.-C.; Junker, R.R.; Hölbling, D. Evolution of debris cover on glaciers of the Eastern Alps, Austria, between 1996 and 2015. *Earth Surf. Process. Landf.* **2021**, *46*, 1673–1691. [CrossRef]

23. Gibson, M.J.; Glasser, N.F.; Quincey, D.J.; Mayer, C.; Rowan, A.V.; Irvine-Fynn, T.D. Temporal variations in supraglacial debris distribution on Baltoro Glacier, Karakoram between 2001 and 2012. *Geomorphology* **2017**, *295*, 572–585. [CrossRef]

24. Goodsell, B.; Hambrey, M.J.; Glasser, N.F. Debris transport in a temperate valley glacier: Haut Glacier d'Arolla, Valais, Switzerland. *J. Glaciol.* **2005**, *51*, 139–146. [CrossRef]

25. Rabatel, A.; Letréguilly, A.; Dedieu, J.-P.; Eckert, N. Changes in glacier equilibrium-line altitude in the western Alps from 1984 to 2010: Evaluation by remote sensing and modeling of the morpho-topographic and climate controls. *Cryosphere* **2013**, *7*, 1455–1471. [CrossRef]

26. Žebre, M.; Colucci, R.R.; Giorgi, F.; Glasser, N.F.; Racoviteanu, A.E.; Del Gobbo, C. 200 years of equilibrium-line altitude variability across the European Alps (1901–2100). *Clim. Dyn.* **2021**, *56*, 1183–1201. [CrossRef]

27. Østrem, G. Ice Melting under a Thin Layer of Moraine, and the Existence of Ice Cores in Moraine Ridges. *Geogr. Ann.* **1959**, *41*, 228–230. [CrossRef]

28. Whalley, W.B.; Martin, H.E. Rock glaciers: II models and mechanisms. *Prog. Phys. Geogr.* **1992**, *16*, 127–186. [CrossRef]

29. Gómez, A.; Palacios, D.; Luengo, E.; Tanarro, L.M.; Schulte, L.; Ramos, M. Talus instability in a recent deglaciation area and its relationship to buried ice and snow cover evolution (Picacho del Veleta, Sierra Nevada, Spain). *Geogr. Ann. Ser. A Phys. Geogr.* **2003**, *85*, 165–182. [CrossRef]

30. Kellerer-Pirklbauer, A.; Kaufmann, V. Deglaciation and its impact on permafrost and rock glacier evolution: New insight from two adjacent cirques in Austria. *Sci. Total Environ.* **2018**, *621*, 1397–1414. [CrossRef] [PubMed]

31. Berthling, I. Beyond confusion: Rock glaciers as cryo-conditioned landforms. *Geomorphology* **2011**, *131*, 98–106. [CrossRef]

32. Shroder, J.F.; Bishop, M.P.; Copland, L.; Sloan, V.F. Debris-covered glaciers and rock glaciers in the nanga parbat himalaya, pakistan. *Geogr. Ann. Ser. A Phys. Geogr.* **2000**, *82*, 17–31. [CrossRef]

33. Monnier, S.; Kinnard, C. Reconsidering the glacier to rock glacier transformation problem: New insights from the central Andes of Chile. *Geomorphology* **2015**, *238*, 47–55. [CrossRef]

34. Monnier, S.; Kinnard, C. Pluri-decadal (1955–2014) evolution of glacier–rock glacier transitional landforms in the central Andes of Chile (30–33° S). *Earth Surf. Dynam.* **2017**, *5*, 493–509. [CrossRef]

35. Jones, D.B.; Harrison, S.; Anderson, K.; Whalley, W.B. Rock glaciers and mountain hydrology: A review. *Earth Sci. Rev.* **2019**, *193*, 66–90. [CrossRef]

36. Ackert, R.P., Jr. A rock glacier/debris-covered glacier system at galena creek, Absaroka mountains, Wyoming. *Geogr. Ann. Ser. A Phys. Geogr.* **1998**, *80*, 267–276. [CrossRef]

37. Anderson, R.S.; Anderson, L.S.; Armstrong, W.H.; Rossi, M.W.; Crump, S.E. Glaciation of alpine valleys: The glacier—Debris-covered glacier—Rock glacier continuum. *Geomorphology* **2018**, *311*, 127–142. [CrossRef]

38. Buckel, J.; Otto, J.-C. The Austrian Glacier Inventory GI 4 (2015) in ArcGis (shapefile) format, supplement to: Buckel, Johannes; Otto, Jan-Christoph; Prasicek, Günther; Keuschnig, Markus (2018): Glacial lakes in Austria—Distribution and formation since the Little Ice Age. *Glob. Planet. Chang.* **2018**, *164*, 39–51. [CrossRef]

39. Wagner, T.; Ribis, M.; Kellerer-Pirklbauer, A.; Krainer, K.; Winkler, G. The Austrian rock glacier inventory RGI_1 and the related rock glacier catchment inventory RGCI_1 in ArcGis (shapefile) format. *PANGAEA* **2020**. [CrossRef]

40. Fischer, A.; Seiser, B.; Stocker-Waldhuber, M.; Mitterer, C.; Abermann, J. The Austrian Glacier Inventories GI 1 (1969), GI 2 (1998), GI 3 (2006), and GI LIA in ArcGIS (shapefile) format, supplement to: Fischer, A.; Seiser, B.; Stocker-Waldhuber, M.; Mitterer, C.; Abermann, J. (2015): Tracing glacier changes in Austria from the Little Ice Age to the present using a lidar-based high-resolution glacier inventory in Austria. *Cryosphere* **2015**, *9*, 753–766.

41. GBA. *GEOFAST—Zusammenstellung Ausgewählter Archivunterlagen der Geologischen Bundesanstalt 1:50.000—146 Oetz*; Verlag der Geologischen Bundesanstalt: Wien, Austria, 2011.

42. MacGlone, J.C. *Manual of Photogrammetry*, 5th ed.; American Society for Photogrammetry and Remote Sensing: Bethesda, MD, USA, 2004; ISBN 1570830711.

43. Glira, P.; Pfeifer, N.; Briese, C.; Ressl, C. A Correspondence Framework for ALS Strip Adjustments based on Variants of the ICP Algorithm Korrespondenzen für die ALS-Streifenausgleichung auf Basis von ICP. *Photogramm. Fernerkund. Geoinf.* **2015**, *2015*, 275–289. [CrossRef]

44. Pfeifer, N.; Mandlburger, G.; Otepka, J.; Karel, W. OPALS—A framework for Airborne Laser Scanning data analysis. *Comput. Environ. Urban Syst.* **2014**, *45*, 125–136. [CrossRef]

45. Petrini-Monteferri, F.; Wichmann, V.; Georges, C.; Mantovani, D.; Stötter, J. Erweiterung der GIS Software SAGA zur Verarbeitung von Laserscanning-Daten der Autonomen Provinz Bozen-Südtirol. In *Angewandte Geoinformatik 2009: Beiträge zum 21. AGIT-Symposium Salzburg*; Strobl, J., Blaschke, T., Eds.; Wichmann: Heidelberg, Germany, 2009; pp. 47–52.

46. Conrad, O.; Bechtel, B.; Bock, M.; Dietrich, H.; Fischer, E.; Gerlitz, L.; Wehberg, J.; Wichmann, V.; Böhner, J. System for Automated Geoscientific Analyses (SAGA) v. 2.1.4. *Geosci. Model Dev.* **2015**, *8*, 1991–2007. [CrossRef]

47. Nuth, C.; Kääb, A. Co-registration and bias corrections of satellite elevation data sets for quantifying glacier thickness change. *Cryosphere* **2011**, *5*, 271–290. [CrossRef]

48. McNabb, R. Pybob. 2019. Available online: https://pybob.readthedocs.io/en/stable/ (accessed on 10 October 2022).

49. Anderson, S.W. Uncertainty in quantitative analyses of topographic change: Error propagation and the role of thresholding. *Earth Surf. Process. Landf.* **2019**, *44*, 1015–1033. [CrossRef]

50. Fleischer, F.; Haas, F.; Altmann, M.; Rom, J.; Knoflach, B.; Becht, M. Combination of historical and modern data to decipher the geomorphic evolution of the Innere Ölgruben rock glacier, Kaunertal, Austria, over almost a century (1922–2021). *Permafr. Periglac.* **2022**, *34*, 3–21. [CrossRef]

51. Fleischer, F.; Haas, F.; Piermattei, L.; Pfeiffer, M.; Heckmann, T.; Altmann, M.; Rom, J.; Stark, M.; Wimmer, M.H.; Pfeifer, N.; et al. Multi-decadal (1953–2017) rock glacier kinematics analysed by high-resolution topographic data in the upper Kaunertal, Austria. *Cryosphere* **2021**, *15*, 5345–5369. [CrossRef]

52. Paul, F.; Barrand, N.E.; Baumann, S.; Berthier, E.; Bolch, T.; Casey, K.; Frey, H.; Joshi, S.P.; Konovalov, V.; Le Bris, R.; et al. On the accuracy of glacier outlines derived from remote-sensing data. *Ann. Glaciol.* **2013**, *54*, 171–182. [CrossRef]

53. Abermann, J.; Fischer, A.; Lambrecht, A.; Geist, T. On the potential of very high-resolution repeat DEMs in glacial and periglacial environments. *Cryosphere* **2010**, *4*, 53–65. [CrossRef]

54. Fischer, A.; Schwaizer, G.; Seiser, B.; Helfricht, K.; Stocker-Waldhuber, M. High-resolution inventory to capture glacier disintegration in the Austrian Silvretta. *Cryosphere* **2021**, *15*, 4637–4654. [CrossRef]

55. Klug, C.; Bollmann, E.; Galos, S.P.; Nicholson, L.; Prinz, R.; Rieg, L.; Sailer, R.; Stötter, J.; Kaser, G. Geodetic reanalysis of annual glaciological mass balances (2001–2011) of Hintereisferner, Austria. *Cryosphere* **2018**, *12*, 833–849. [CrossRef]

56. Smith, M.J.; Clark, C.D. Methods for the visualization of digital elevation models for landform mapping. *Earth Surf. Process. Landf.* **2005**, *30*, 885–900. [CrossRef]

57. Kenner, R.; Noetzli, J.; Hoelzle, M.; Raetzo, H.; Phillips, M. Distinguishing ice-rich and ice-poor permafrost to map ground temperatures and ground ice occurrence in the Swiss Alps. *Cryosphere* **2019**, *13*, 1925–1941. [CrossRef]

58. McNabb, R.; Nuth, C.; Kääb, A.; Girod, L. Sensitivity of glacier volume change estimation to DEM void interpolation. *Cryosphere* **2019**, *13*, 895–910. [CrossRef]

59. Kääb, A. Glacier Volume Changes Using ASTER Satellite Stereo and ICESat GLAS Laser Altimetry. A Test Study on EdgeØya, Eastern Svalbard. *IEEE Trans. Geosci. Remote Sens.* **2008**, *46*, 2823–2830. [CrossRef]

60. Helfricht, K.; Huss, M.; Fischer, A.; Otto, J.-C. Spatial ice thickness distribution and glacier bed elevation for glaciers of the third Austrian Glacier Inventory (GI3), supplement to: Helfricht, K.; Huss, M.; Fischer, A.; Otto, J.-C. (2019): Calibrated Ice Thickness Estimate for All Glaciers in Austria. *Front. Earth Sci.* **2019**, *7*, 68. [CrossRef]

61. Huss, M.; Farinotti, D. Distributed ice thickness and volume of all glaciers around the globe. *J. Geophys. Res.* **2012**, *117*, F04010. [CrossRef]

62. Scambos, T.; Dutkiewicz, M.; Wilson, J.; Bindschadler, R. Application of image cross-correlation to the measurement of glacier velocity using satellite image data. *Remote Sens. Environ.* **1992**, *42*, 177–186. [CrossRef]

63. Fey, C.; Krainer, K. Analyses of UAV and GNSS based flow velocity variations of the rock glacier Lazaun (Ötztal Alps, South Tyrol, Italy). *Geomorphology* **2020**, *365*, 107261. [CrossRef]

64. Seppi, R.; Carturan, L.; Carton, A.; Zanoner, T.; Zumiani, M.; Cazorzi, F.; Bertone, A.; Baroni, C.; Salvatore, M.C. Decoupled kinematics of two neighbouring permafrost creeping landforms in the Eastern Italian Alps. *Earth Surf. Process. Landf.* **2019**, *44*, 2703–2719. [CrossRef]

65. Helfricht, K.; Huss, M.; Fischer, A.; Otto, J.-C. Calibrated Ice Thickness Estimate for All Glaciers in Austria. *Front. Earth Sci.* **2019**, *7*, 68. [CrossRef]

66. Noetzli, J.; Hoelzle, M.; Haeberli, W. Mountain permafrost and recent Alpine rock-fall events: A GIS-based approach to determine critical factors. In Proceedings of the Eighth International Conference on Permafrost, Zürich, Switzerland, 21–25 July 2003; Volume 2, pp. 827–832.

67. Ravanel, L.; Magnin, F.; Deline, P. Impacts of the 2003 and 2015 summer heatwaves on permafrost-affected rock-walls in the Mont Blanc massif. *Sci. Total Environ.* **2017**, *609*, 132–143. [CrossRef]

68. Kirkbride, M.P.; Deline, P. The formation of supraglacial debris covers by primary dispersal from transverse englacial debris bands. *Earth Surf. Process. Landf.* **2013**, *38*, 1779–1792. [CrossRef]

69. Mölg, N.; Ferguson, J.; Bolch, T.; Vieli, A. On the influence of debris cover on glacier morphology: How high-relief structures evolve from smooth surfaces. *Geomorphology* **2020**, *357*, 107092. [CrossRef]

70. Westoby, M.J.; Rounce, D.R.; Shaw, T.E.; Fyffe, C.L.; Moore, P.L.; Stewart, R.L.; Brock, B.W. Geomorphological evolution of a debris-covered glacier surface. *Earth Surf. Process. Landf.* **2020**, *45*, 3431–3448. [CrossRef]

71. Mears, B. Periglacial Wedges and the Late Pleistocene Environment of Wyoming's Intermontane Basins. *Quat. Res.* **1981**, *15*, 171–198. [CrossRef]

72. Kneisel, C. Permafrost in recently deglaciated glacier forefields—Measurements and observations in the eastern Swiss Alps and northern Sweden. *Z. Geomorphol.* **2003**, *47*, 289–305. [CrossRef]

73. Kneisel, C.; Kääb, A. Mountain permafrost dynamics within a recently exposed glacier forefield inferred by a combined geomorphological, geophysical and photogrammetrical approach. *Earth Surf. Process. Landf.* **2007**, *32*, 1797–1810. [CrossRef]

74. Muller, S. *Permafrost or Permanently Frozen Ground and Related Engineering Problems*; J.W. Edwards: Ann Arbor, MI, USA, 1947.

75. Van Everdingen, R. *Multi-Language Glossary of Permafrost and Related Ground-Ice Terms*; The University of Calgary: Calgary, AB, USA, 1989.

76. Harris, C. Permafrost. In *Encyclopedia of Geomorphology*; Goudie, A., Ed.; Routledge: London, UK; New York, NY, USA, 2004; pp. 777–779.

77. Haeberli, W. Modern Research Perspectives Relating to Permafrost Creep and Rock Glaciers: A Discussion. *Permafrost Periglac. Process.* **2000**, *11*, 290–293. [CrossRef]

78. Draebing, D.; Mayer, T.; Jacobs, B.; McColl, S.T. Alpine rockwall erosion patterns follow elevation-dependent climate trajectories. *Commun. Earth Environ.* **2022**, *3*, 21. [CrossRef]

79. Petersen, E.I.; Levy, J.S.; Holt, J.W.; Stuurman, C.M. New insights into ice accumulation at Galena Creek Rock Glacier from radar imaging of its internal structure. *J. Glaciol.* **2020**, *66*, 1–10. [CrossRef]

80. Azizi, F.; Whalley, W. Finite Element Analysis of the Creep of Debris Containing Thin Ice Bodies. In Proceedings of the Fifth (1995) International Offshore and Polar Engineering Conference, The Hague, The Netherlands, 11–16 June 1995; pp. 336–341.

81. Moore, P.L. Deformation of debris-ice mixtures. *Rev. Geophys.* **2014**, *52*, 435–467. [CrossRef]